Virtual Inspection of Additively Manufactured Parts

Pavol Klacansky* SCI Institute University of Utah
Haichao Miao† LLNL
Attila Gyulassy‡ SCI Institute University of Utah
Andrew Townsend§ LLNL
Kyle Champley¶ LLNL
Joseph Tringe‖ LLNL
Valerio Pascucci** SCI Institute University of Utah
Peer-Timo Bremer†† LLNL

ABSTRACT

Advanced manufacturing techniques, such as additive manufacturing, enable the design of increasingly complex components for a wide range of industrial applications. However, this complexity makes qualification of the parts, determining whether a part is within some margin of error from the initial design, difficult. To inspect and qualify complex internal geometries that are not accessible with an external probe, parts are typically scanned with computed tomography (CT), and manually compared to the computer-aided design (CAD) model using visual inspections. Matching the CAD model to the 3D reconstructed object is challenging in a traditional desktop environment due to the lack of depth perception and 3D interaction. An additional challenge comes from the geometric complexity of CAD meshes and large-scale CT scans. We present a virtual reality (VR) system for manual qualification, providing a novel defect visualization method. First, we describe a semiautomatic *CAD-to-Scan Registration* approach in VR using a finite element mesh. Second, we introduce the *Defect Box*, which enables full-resolution inspection for massive scans and CAD-CT comparison of local defect regions. Finally, our system includes intuitive *3D Metrology* methods that enable natural interactions for the measurement of features and defects in VR. We demonstrate our approach on both real and synthetic data and discuss feedback from four expert users in nondestructive qualification.

Index Terms: Human-centered computing—Visualization—Visualization systems and tools; Human-centered computing—Visualization—Visualization application domains—Scientific visualization; Human-centered computing—Visualization—Empirical studies in visualization

1 INTRODUCTION

3D printing and similar techniques are revolutionizing manufacturing. These so-called *additive manufacturing* techniques can create intricate truss structures, internal density gradients, and a host of other complex features that are difficult and often impossible to produce with traditional approaches [32]. However, additive manufacturing involves nascent technology that can result in unexpected defects [31], such as internal voids, broken or missing features, or superfluous material, all of which can significantly impact the performance of the resulting part. Consequently, verifying that a given part meets its specification is crucial to both improve the manufacturing process and confidently use the resulting components. In traditional manufacturing, this verification step can be performed through high-resolution surface scans or by using high-precision physical probes. Unfortunately, these techniques cannot assess complex, internal features and thus are of limited use for many additively manufactured parts. Furthermore, the large variability between prints and the high cost in both time and money to print a novel part make destructive evaluation unattractive. Instead, the field is moving toward *computer-supported inspection* in which high-resolution computed tomography (CT) scans (or other modalities such as neutron scans or ultrasound) are used to assess the quality of a given build.

Although conceptually simple and powerful, virtual inspections are creating their own challenges. First, the scans are often large, with modern scanners producing volumes in excess of $4K^3$ voxels and over 200 GB for a single measurement modality. Furthermore, these scans are processed on a workstation because the target audience has limited access and no practical experience with parallel computing and the corresponding tools. Second, the scanning and reconstruction process introduces its own artifacts, especially in dense metal objects, creating volumes that are difficult to segment automatically. Notably, there can exist significant local and global drifts in value making a global isosurface an unsuitable representation of the boundary surface of the object [19]. Other artifacts, such as streaks, further complicate the surface extraction. Finally, at the cutting edge of additive manufacturing of interest to our collaborators, components are often individually designed and printed in very limited numbers or are even unique, rendering the development of a specialized, automatic inspection pipeline impractical. Instead, much of the current inspection process is performed manually, with scientists visualizing a given scan to check for defects, and if necessary, developing custom analysis routines to quantify features of interest. This process is not only time-consuming and error prone, but it is also rapidly reaching practical limits because the sheer data sizes are overwhelming existing tools, and the complexity of parts defies manual inspection using traditional desktop applications. For example, performing measurements of struts in truss structures is difficult because these struts may not lie on axis-aligned planes. Measuring the width of these struts would require the placement on an non-axis-aligned plane. In virtual reality (VR), taking measurements in arbitrary orientations is natural [13, 16, 23].

We present a virtual-reality-based system that significantly simplifies the overall process by providing an intuitive approach to directly compare the computed-aided design (CAD) model of the as-designed part with the CT scan of the corresponding physical object. Using natural gestures and interaction patterns, our *CAD-to-Scan Registration* enables a fast manual alignment of the CAD model with an isosurface-based representation. This initial alignment can be further improved by offline registration tools. Subsequently, we propose a *Defect Box* visualization approach that allows detailed examination of defects using a combination of slicing and local surface rendering techniques to help users explore differences between the as-designed and as-built part. Exploiting progressive, multiresolution data layouts [35], the system can natively handle even the largest scans. This multiresolution data layout was used,

*e-mail: klacansky@sci.utah.edu
†e-mail: miao1@llnl.gov
‡e-mail: jediati@sci.utah.edu
§e-mail: townsend10@llnl.gov
¶e-mail: champley1@llnl.gov
‖e-mail: tringe2@llnl.gov
**e-mail: pascucci@sci.utah.edu
††e-mail: bremer5@llnl.gov

2022 IEEE 15th Pacific Visualization Symposium (PacificVis) | 978-1-6654-2335-9/22/$31.00 ©2022 IEEE | DOI: 10.1109/PACIFICVIS53943.2022.00017

2165-8773/22/$31.00 ©2022 IEEE
DOI 10.1109/PacificVis53943.2022.00017

for example, to analyze the results of a large-scale climate simulation [7]. The immersive visualization and interaction makes taking measurements for *3D Metrology* applications straightforward. Based on expert feedback, the immersive 3D rendering and interaction is more effective than the traditional screen and mouse approach of existing tools. We present the following contributions:

- A problem characterization of the virtual analysis and measurement of large-scale CT scans and CAD models from the perspective of visualization.
- A VR system for inspection of complex parts that includes a novel *CAD-to-Scan Registration* and *3D Metrology* approach.
- A specialized local defect visualization method (*Defect Box*) that incorporates familiar desktop-based inspection approaches to a VR environment.
- A set of publicly available synthetic datasets with example defects for validating automated defect detection and visualization tools.

2 Background

Fabrication of novel parts relies on the ability of experts to visually inspect defects. The workflow begins with the creation of a CAD model, which is then additively manufactured and scanned with a high-resolution CT system. The resulting scan is a 3D reconstruction of the CT data. Nondestructive evaluation is usually performed using 2D slices of the reconstructed 3D volume, whereas the CAD model is used as a reference.

Generating the CAD model, essentially a high polygon count triangle mesh, requires intricate understanding of the additive manufacturing process and the purpose of the targeted physical object. Tools, such as nTopology [1], help generate structures with the desired physical properties, including manufacturability.

Additive manufacturing processes have enabled the creation of metal components with highly complex internal geometries and unique physical properties, such as high specific strength and stiffness. Our collaborators often create lattice structures that are composed of repeated unit cells. These structures have intricate details and allow design freedom beyond the capabilities of solid materials [32]. Due to the control of the physical properties and shapes, these lattice structures have shown great potential in medical [43], aviation, and aerospace [53] applications. The individual unit cells of a lattice structure consist of struts that form different topological arrangements, such as an octet (Fig. 1a), which is also used in the datasets in this paper. Defects are often associated with added or missing material on the struts [31]. Detecting and classifying these defects is crucial; therefore, we modeled a set of example defects for validation purposes (Fig. 1). Furthermore, we generated the corresponding volumetric datasets using a physics-based CT reconstruction tool [6].

The current analysis workflow relies on inspecting 2D slices, which requires increased cognitive effort to mentally reconstruct the 3D object. Furthermore, performing 3D measurements on axis-aligned slices is even more challenging as features and defects are usually not located on an axis-aligned slice. Another challenge is imposed by the 2D desktop screen because viewing complex structures is difficult due to inaccurate depth perception. Although CAD-to-Scan Registration is crucial for defect analysis, the experts face the problem of time-consuming interaction with 3D models. Yet, understanding the deviations of the CT volume from the CAD model is necessary for both qualification of the manufactured part and developing and improving the manufacturing process itself.

3 Related Work

We discuss the applications of VR to scientific visualization and a set of frameworks and systems to guide and simplify development of such visualization tools.

3.1 VR Visualization Applications

Research studies have demonstrated that VR can increase productivity and lead to new insights, such as in neuroscience [4,37,41,47,49], biology [10,36], visualization of trajectories [8,18], atomistic simulations [39], radiology [44], surgical planning [40], or graph visualization [17,25]. Additionally, the Cave Automatic Virtual Environment (CAVE) [9] has been applied to visualize potential factory improvements [51]. For example, the system was used to view the noise levels in a factory or equipment changes at the human scale.

The 3D Visualizer [23] is one of the first VR visualization tools that supports measuring distances and angles and marking regions of interest. It is built using the Vrui toolkit for rapid VR application development [22]. The system's responsiveness is maintained by performing only a part of the work each frame and incrementally constructing the output, e.g., an isosurface, over multiple frames. The isosurface algorithm proposed is progressive [50] and can be seeded by pointing a controller at a function value, for example, on a slice. This system supports a variety of devices, such as CAVE [9], head-mounted displays, or the Virtual Workbench [12,34]. Moreover, the interactive tool for protein manipulation [24] has been extended to the VR environment [21] using this framework, and an informal study showed a decrease in the training required to use this tool compared to its desktop counterpart because of the direct manipulation of protein substructures in 3D space. We do not use Vrui toolkit because it does not support large-scale datasets.

A virtual laboratory [13,16] is a virtual environment where scientists can inspect, measure, and analyze their datasets. The laboratory was primarily designed to support inspection of scaffold structures in tissue engineering. The preliminary versions of this laboratory supported length and volume measurements and the ability to plot these measurements as histograms. The exploration of the data was enhanced by plane and box clipping tools. Traditional desktop graphical user interfaces and selection modes were used to interact with the measuring tools. Unfortunately, the supported datasets are required to be polygonal meshes, and the tool is not designed to handle large-scale volumetric datasets. More importantly, comparison, deformation, and interaction with two different modalities (CT and CAD) are not directly supported, and thus the tool is unsuitable for qualification of manufactured parts.

Length, angle, and volume measurements are an important part of surgical planning, and desktop tools were developed to perform these measurements directly on a desktop screen using perspective projection and 2D view [38]. Furthermore, if a dataset is already segmented, automatic measurements of object's extent can be calculated with principal component analysis. These desktop tools were extended to a VR environment [40], resulting in reduced time needed to perform volume measurements. The distance measurements took approximately the same time as on a desktop; however, the VR environment was preferred by most users.

Data visceralization [28] is a technique to use VR for conveying physical phenomena, such as distance, speed, height, and scale, and abstract concepts, such as national debt. In the data visceralization user study, VR visualizations were preferred for observing physical phenomena (speed and height) compared to the abstract concept of money. Moreover, annotations were useful to augment the visual information without distracting the users, and it may be preferable to prepare a set of viewpoints to avoid a user missing an important information. The results suggest the application of VR to metrology may be preferable, and future examples of visual inspection reports should save viewpoints at which the measurements were made.

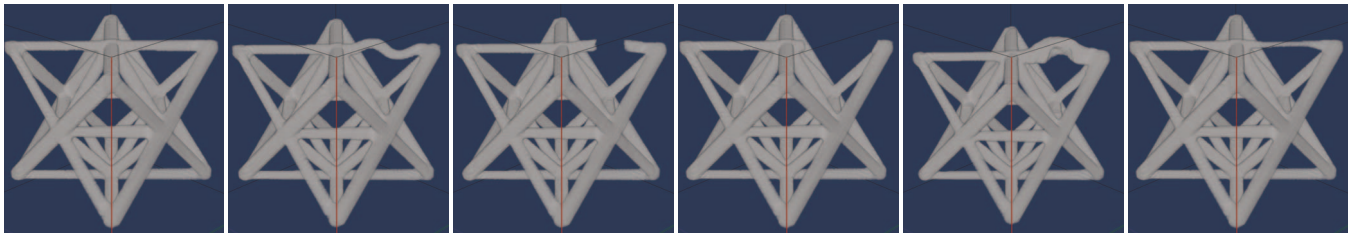

(a) No defect. (b) Bent strut. (c) Broken strut. (d) Missing strut. (e) Dross defect. (f) Thin strut.

Figure 1: We simulated an octet truss unit cell with five geometric defects. A physics-based CT reconstruction tool [6] was used to simulate these synthetic scans. The material used is Ti-6Al-4V, and the datasets are 256^3 in size. All defects are manually introduced at the same location. During analysis, these defects are of particular interest because they have an adverse effect on the overall strength and stiffness of the structure. Fig. 1a shows an octet truss unit cell without any defects. The strut direction can potentially result in bending (Fig. 1b). The bending can be followed by a fracture, resulting in a broken (Fig. 1c) or entirely missing (Fig. 1d) strut. Other discrepancies between the CAD model and the manufactured part are a buildup of additional material, called a dross defect (Fig. 1e), or a lack of material, resulting in thin struts (Fig. 1f). The CAD models and the corresponding volumes are available at `https://data-science.llnl.gov/open-data-initiative`.

3.2 VR Frameworks and Systems

The immersive metrology framework [5] is an approach to develop and evaluate immersive metrology tools. The framework consists of five stages: literature review, assessment of current technology, identification of components of an interface, development of a prototype, and, finally, analysis of the results. The authors of this framework propose a pre-test to familiarize the participants with the technology, and the main test to assemble a satellite module and verify the correctness of the assembly by performing measurements. This assembly would require prior experience, needs to be accurate, and would replicate an industrial application. Unfortunately, no applications of this framework were presented in this study, and suitability of this approach to our use case is unclear.

The traditional game engines, such as Unreal Engine or Unity3D, support VR rendering. However, research is ongoing into designing rapid prototyping environments specialized for visualization. For example, scenery [15] is a framework for building data visualizations in VR and CAVE systems utilizing the Java virtual machine, which enables an easy integration with other popular tools written in Java, such as the image processing software Fiji [42], at the cost of incompatibility with C++ libraries, e.g., MFEM [3], we use to represent deformations. The framework supports out-of-core rendering and provides both OpenGL and Vulkan rendering backends for multiplatform applications. To render and composite multiple overlapping datasets in a single view, the framework generates the shader programs dynamically depending on the scene. To handle large data, it relies on an image pyramid in contrast to our data reorganization via the IDX format [35]. Other systems, such as Flex-ER [29], propose a JSON-based descriptive language for creating immersive analytics visualizations compatible with virtual and augmented reality. This system automatically supports user study trials and thus is suitable for comparison between different devices, e.g., a tablet and VR headset. A text file describes the configuration of the experiment as well as its state machines to handle the interactions. However, the supported interactions are limited to brushing and selection, and therefore they are not suitable for interacting with complex objects as enabled by our inspection system.

3.3 Defect Visualization in Large-Scale Volumes

Local defects occupy only a small fraction of the entire volume, and focus+context methods [45] are natural candidates for visualizing these details at full resolution, whereas the entire structure is depicted at low resolution. Interactive lenses [33] are typical examples of such techniques with which we locally embed a higher detailed view. However, due to the 3D nature of the data and the resulting occlusion issues [11], we choose to displace the focus region and enlarge it. Inside this region, we load the selected subset of a dataset at full resolution and render its isosurfaces.

A recent study [52] has compared room-scale overview+detail paradigm with zooming in three tasks on 3D scatterplots: comparing distances of close points, comparing distances of far points, and comparing point cluster sizes. In contrast to this work, we know the regions of interest and do not use overview to navigate the dataset. We use overview (minimap) to select defects for detailed inspection and to gain a high-level understanding of the defect locations.

The fidelity of isosurfaces in VR has been investigated [26] and compared to volume rendering [27], suggesting that isosurfaces generally benefit more from stereo viewing. However, isosurfaces are often not suitable to capture global boundary surface in CT scans because the function values vary due to high metal occlusion, drifts, or streaks. Localized techniques can be used to extract an accurate global surface [19]. We use small regions capturing defects where the value drift is expected to be small, and isosurfaces, especially with adjustable isovalues, are sufficient.

4 Domain Objectives and Challenges

The described work is part of a larger effort to improve the analysis and quantification in the nondestructive evaluation of complex parts. As part of the interdisciplinary team of scientists, we are responsible for solving the urgent needs in the analysis of deviations of the CT scan from the CAD model. Over the course of the past 14 months, we participated in weekly meetings with the relevant subteams. Being embedded in this project has enabled us to obtain a thorough understanding of the domain background, its challenges and goals. This close participation ensured that our developed approach meets their needs, and the collaboration allowed us to gather their ideas early on. In reports and presentations, we regularly demonstrate the progress and incorporate their suggestions.

Codesign of Prototype The collaboration started by investigating an application of VR to inspection of scans of manufactured parts. We built a prototype tool that could display small-scale datasets using isosurfaces, allowed object manipulation, and provided methods for measuring distances and angles and marking defects. Various experts tested this prototype and provided us with valuable input that we used in future iterations. The goal of the initial prototype was to answer two questions: i) does VR help with understanding the component structure and its defects, and ii) can we build an intuitive interface and interactions for domain experts to effectively inspect these datasets. We learned that local defects are often quite small relative to the size of the part. We observed that scaling up the object and immersing users in the dense volume cause nausea, mostly due to disorientation. Another problem with the magnified view is that

rotations around the controller axis induce large rotations in the periphery. Finally, the experts raised the issue of needing to visualize large scans, plot values alongside a line segment, and visualize and register CAD meshes.

Informed by the prototype and feedback from our collaborators, we focus on one of the main bottlenecks of advancing both the manufacturing methods and the nondestructive evaluation techniques, the ability to understand how the as-built part deviates from the initial design. In this context, we have distilled the following goals:

G-1 **Visualize Large-Scale CT and CAD in the Same Space.** The experts would like to view the 3D structure of the CAD model and the large-scale CT scan in the same environment interactively and intuitively.

G-2 **Validate CT Scan.** CT produces a series of images that are used to reconstruct the volume. Understanding the structure and the defects in the as-built part is important to adjust the scanner and reconstruction parameters, which can be changed to reduce artifacts and increase fidelity of the scan.

G-3 **Align CT with CAD Model.** To study the differences between the as-built and the as-designed part, it is necessary to align the scan and the model. Typically, the initial alignment is performed manually, and then it is refined by an automated tool. The result of this automated registration needs to be visualized to detect obvious deviations, which potentially correspond to defects.

G-4 **Inspect and Quantify Defects.** Defects are likely small and inside a volume and may be visually occluded. We need a simple way to inspect these defects at the full resolution of the volume. We have to take the locality of defects into account as some defect are invisible at reduced resolutions.

5 Design of Virtual Reality Inspection System

We have designed a set of interactions coupled with the application of a finite element mesh to represent global deformations introduced by the printing process, representing the *CAD-to-Scan Registration*. Furthermore, we add a two-level focus+context inspection tool consisting of a low-fidelity view, a *Minimap*, serving to navigate between individual defects, and a high-fidelity *Defect Box* for inspection of a selected defect. Finally, we designed a 3D Metrology approach to measure lengths, angles, and density profiles for the *Defect Box*.

5.1 Visualization and CAD-to-Scan Registration

The CAD model is essentially the idealized version of the scan. Direct comparison with CAD can reveal deviations, which in turn are likely to be defects. Alignment of the CAD to the scan reduces the complex task of defect inspection to a search for deviations. Due to potential printing artifacts like sagging or twisting, we expect an optimal registration to require a complex, nonlinear, and potentially local transformation to map the as-designed CAD mesh to the as-measured CT scan. A fully automatic, nonlinear registration represents a significant challenge and is beyond the scope of this paper. However, the first step in many iterative techniques, like the one used here, is to provide a good initial alignment, and we find the intuitive object manipulation and visualization in VR to be particularly effective for this task (G-3). The manual registration proceeds in two steps (Fig. 2): an initial rigid body transformation by simultaneously moving and scaling both objects, and fine-scale adjustments through manipulation of the deformation mesh. The final registration uses an offline iterative technique that is not fully completed, and thus it is not part of the presented system.

Interaction. Objects, such as a CT scan or CAD model, have their bounding boxes rendered and can be manipulated by the user. The manipulation operations support exploration and registration using translation, rotation, and scaling. The scaling operation uses the metaphor of moving the controllers closer together [21] and is proportional to the distance between the controllers. We plan to investigate adding translation and rotation during scaling to keep the controllers latched to their grab locations [52]. A controller is associated with an object on a trigger press, instead of a frame-by-frame test of the object under the controller's pointer. We found the latter method would produce an incorrect selection if a frame is missed or the controller temporarily loses tracking. If objects overlap, the object selection is resolved in a fixed order, prioritizing the deformation mesh control points, then the CAD model, and finally the CT scan. To aid a user with the selection, the hovered object is highlighted by rendering its bounding box in white, and the controller vibrates briefly. The objects can be positioned independently; for example, the left controller can manipulate the CAD model while the right controller is used to move the CT scan.

Nonrigid Alignment. The printing process often introduces both local and global defects beyond what can be represented through rigid body alignments. Independent of the specific registration technique, the first challenge is to develop a representation for either the CAD mesh or the CT grid that can efficiently encode nonlinear deformations. As visualizing a large-scale warped grid would be significantly more expensive than manipulating a surface representation, we have chosen the CT grid to remain fixed and deform the CAD mesh to match. To this end, we embed the CAD mesh into a volumetric *deformation mesh* implemented in MFEM [3], a finite element mesh library. The deformation mesh is initialized with the bounding box of the CAD mesh and subsequently can be manipulated rigidly as an object or through moving individual control points. At each change, the CAD model is transformed from the parameter space of the deformation mesh to physical space (of the CT grid) for rendering. The initial manual alignment is followed by an offline iterative optimization process that further aligns both objects. Note that the initial alignment is crucial for the iterative process to converge (G-3), and an accurate registration is key to detect local defects such as broken struts without the user being overwhelmed by difference due to, for example, a global twist (G-4). One of the technical challenges is that the direct manipulation of objects through the controller as discussed in the previous section is necessarily approximate as even in VR the user cannot simultaneously see, let alone easily match, all eight corners of a bounding box. Additionally, small involuntary hand movements further complicate an exact alignment. Instead, we allow detailed registration by directly manipulating the control points of the MFEM mesh, deliberately damping the motion to by a linear combination of old and current positions. This dampening causes the manipulated control point to lag behind the controller's motion, evoking the feeling of an attachment by a weak rubber band. Another advantage of this approach is that it hides potential latencies in updating physical coordinates of very large CAD models while moving control points.

Rendering. The rendering system needs to present the CAD and CT objects to the user (G-1). Since the CAD model is a triangle mesh, we use rasterization. For CT scans, we have a choice of ray casting the volume or extracting the surface using the Marching cubes algorithm [30]. We choose the latter due to its simplicity. For the *Minimap* visualization, we subsample the volume [35] to fit it into memory and to reduce the surface size produced by the Marching cubes algorithm. The scene is illuminated by a point light placed at the headset, mimicking a headlamp.

5.2 Local Defect Selection Using Minimap

After the CAD and scan are registered and defects are detected (either manually or automatically), we need a visualization mode

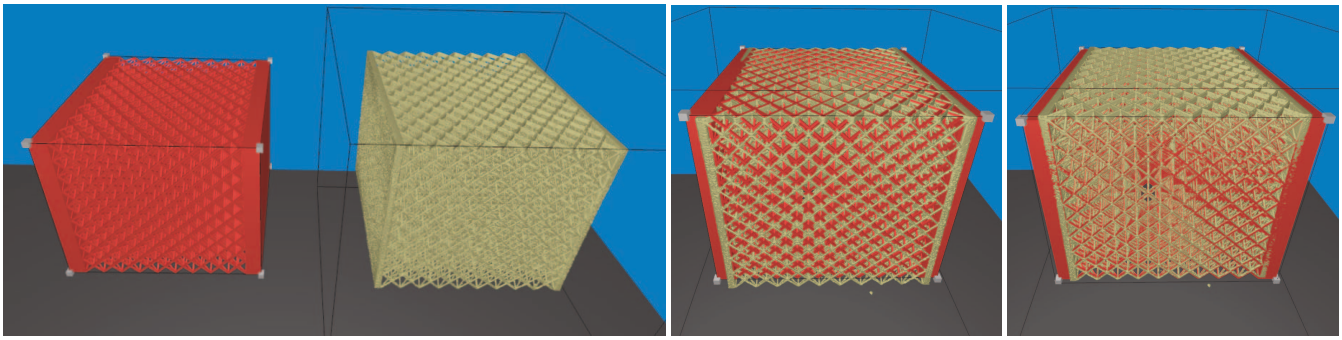

(a) CAD model (red) and CT isosurface (gold) before manual alignment. (b) CAD model aligned by object manipulation. (c) Fine adjustment of CAD model using control points.

Figure 2: Manual registration of the Truss dataset. The alignment process starts by a user manipulating the CAD model (red) and CT scan (gold) objects to obtain approximate alignment (a) and (b). A user can then perform fine adjustments to improve the alignment using the control points (gray cubes) of the deformation mesh (c). Finally, the alignment result can be optionally improved by an offline registration tools.

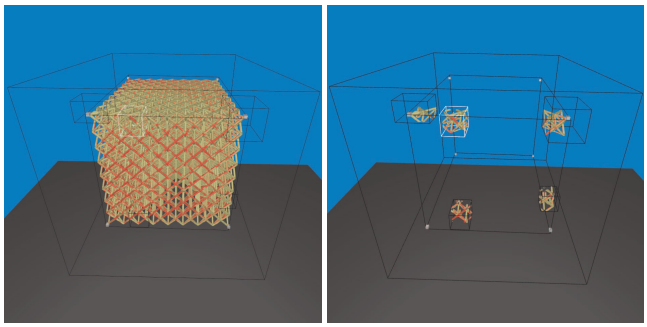

(a) Low-resolution CT isosurface aligned with the CAD. (b) Clipped CAD and CT surfaces in the minimap.

Figure 3: The synthetic truss CAD (red) registered to the simulated CT scan's isosurface (gold). The boxes with defects may be partially or fully occluded by these meshes, and thus we map the menu button to an option to hide everything except the surfaces inside these boxes. The user can reach and select a box with a controller.

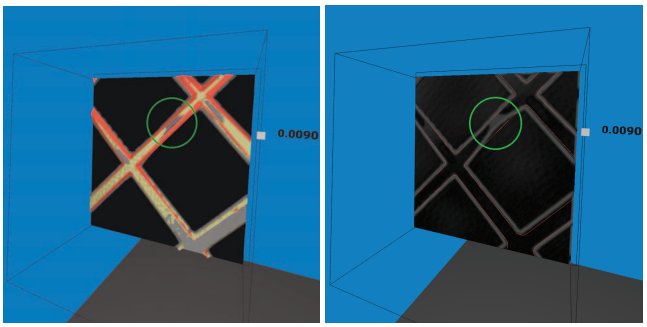

(a) A defect highlighted by clipped CAD and CT. (b) CAD contour and gradient magnitude CT slice.

Figure 4: An inspection of a thin strut in the Synthetic truss dataset using the defect box. The user can adjust the isovalue (in the figure it has a value 0.0090) by moving the gray cube up/down on the right. The defect is highlighted with a green circle. On the left, clipped CAD (red) and isosurface (gold) are shown for user-controllable thickness alongside with the slice displaying the CT values. On the right, the thickness is set to zero, and the slice is set to display the CT gradient magnitude. The red lines correspond to the intersections of the CAD mesh with the slice and help the user validate that these lines map to the high gradient values representing the boundaries. In this view, the user can observe the thin strut present in the CT scan not matching the CAD model.

to obtain an overview of the local defect distribution and to select from the set of all defects. Visualizing local defect distribution can reveal issues in a registration technique, scanning issues, or printing problems. The visualization of CAD and CT after registration serves as a defect minimap that enables quick navigation between individual defects (Fig. 3). This minimap displays the position of boxes containing a defect within the whole dataset. Since these boxes may be internal and obscured by the data, a user has the ability to hide the CAD mesh and isosurface outside these boxes using the controller's menu button. Inside each box in the minimap, we display both isosurface (computed on a lower resolution scan) and clipped CAD mesh because they may help a user to determine defect type. A user can select the content of a defect box from the minimap by placing a controller inside a box with a defect and pressing the trigger button.

5.3 Defect Box for Local Defect Visualization and Metrology

A defect can be local or global. An example of a global defect is twisting of a part, and a local defect can be a broken strut. Local defects are only small in comparison to the entire volume and have to be viewed at full resolution (CT) because some defects are not resolved at reduced resolution (G-4). Furthermore, local defects can be internal to an object, such as the local defects in the Honeycomb dataset (Fig. 6), and geometric occlusion becomes a problem. Moreover, the global isovalue may not be suitable for viewing the local CT due to scanning and reconstruction artifacts, and thus the user needs an option to adjust the isovalue locally. Finally, the inspection of the CT scans (G-2) and quantification of defects require measurements of values, distances, and angles (G-4), potentially on a non-axis-aligned slice.

We present the defect box, an integrated set of tools and visualizations that are necessary to inspect local defects. The defect box displays a portion of a CT scan at full resolution using an isosurface. The isovalue can be adjusted per defect box by moving the slider present on the edge of the box (Fig. 4). A slice is available to inspect either values or gradient magnitude directly (useful for determining boundaries). A user can display the 3D metrology approach at any moment by pressing the Tools button and selecting a tool (Fig. 7). If any of the tools is placed inside the defect box, the transformations of the defect box apply to the tool. This approach enables a user to manipulate the box without tools becoming misaligned. The individual features are discussed below in detail.

Local CAD-to-Scan Comparison. This approach combines a slice with a user-controllable extent of the CAD and CT meshes. It displays the data of the defect box by rendering a slice of function

values or gradient magnitudes (computed using central differences). The gradient magnitude slice is used by the experts to determine the location of the surface boundary in CT scans. The controller's menu button is used to toggle between the two slice views. Initially, the slice position and orientation were tied to that of a controller, but after expert feedback we changed the slice to behave as an object that can be selected and manipulated. Moreover, if the defect box is moved or rotated, the slice is transformed with it. Furthermore, we augment the slice with the ability to display a clipped part of the CAD surface and the isosurface from the CT within a user-controllable thickness. Users can adjust the thickness by scrolling on the controller's trackpad. If the thickness is set to zero, we extract the intersection of the CAD mesh with the slice and display it as contours on the slice. This rendering of the intersection of the CAD mesh with the slice is useful both for validation of the alignment produced by the registration and for defect inspection.

Lineout. We provide a lineout tool that allows a user to place a line segment and plot the CT values as a graph alongside this segment. This capability is useful for determining the boundary of the scanned part (G-3) and inspecting the CT scan (G-2). We sample the graph at a half-voxel rate using trilinear interpolation and offset the rendering of the graph to avoid depth fighting with the line connecting the manipulation points.

Length Measurement. This tool enables the user to measure the length between two manipulation points. Both of these points can be adjusted at the same time with controllers, or the whole tool can be moved by grabbing the line connecting the points. The length is scaled based on the input CT voxel size. Moreover, the displayed unit is automatically adjusted to provide good resolution and avoid flickering (coming from small involuntary hand movements).

Angle Measurement. Angles are measured by moving three manipulation points. Often, it is more convenient to move two points at the same time (since the user has only two hands), and thus we allow the user to move the lines connecting the points.

6 VR Development for Large-scale Volumes

The rendering and interaction latency requirements pose a significant challenge for the development of VR systems, especially when the system needs to query and display datasets in hundreds of gigabytes in size. Our system generates two 1512x1680 images every 11 ms on the laptop used for the case studies, and the response to interactions falls within 100 ms [21] (except for the isosurface update on isovalue change and the deformation mesh update for large CAD meshes).

We build the system in C++ using Direct3D 12 and OpenVR. The choice of C++ is due to the use of external libraries: Eigen [14] for matrix manipulation, MFEM [3] for CAD deformations, and OpenVisus [2] for CT scan data management. We choose Direct3D 12 due to its excellent debugging and profiling tool PIX.

We rely on a job system wherein each frame is scheduled as a separate job. We use atomic counters accompanied by a version number for synchronization between jobs. At any point in time, at least two jobs are in flight: the frame construction job and the rendering job. The frame construction job is responsible for executing user logic and constructing commands for a graphics processor. It may spawn additional jobs to extract an isosurface or compute alignment errors. The rendering job is responsible for submitting the previous frame to a graphics card and then to a VR headset. We query the latest headset position before rendering, minimizing visual latency.

7 Case Studies and Expert Feedback

We present three case studies that demonstrate the usability and effectiveness of our approach. We invited four experts to test the VR system. The purpose of these studies is to find out if the goals described are achieved. In the test sessions, we listened carefully to the users' experiences and observed their performance. In addition, our users are not used to VR devices, and therefore they often had questions about the controls and dropped out of the session. Since our experts do not register the CAD data with the scan on the desktop, we could not make a direct comparison. Therefore, we decided to collect qualitative feedback from the experts while they were using the proposed system to gain additional insights and ideas for improvements. The experts did the case study depending on their availability and focus. For the first case study, the experts performed an interactive CAD-to-Scan Registration on the Truss dataset. For the second case study, the experts analyzed the local defect boxes in the Synthetic truss and Honeycomb datasets. For the last case study, the experts performed metrology on the truss structures.

All four experts are scientists in nondestructive evaluation, but have different backgrounds. The first expert is a group leader primarily interested in a high-level inspection of defects. The second is a scientist, focused on registration, detailed defect analysis, surface texture testing, and measurements. The third expert is a lead tomographic imaging researcher and developer interested in understanding and improving scanning and reconstruction algorithms. The fourth is a senior scientist focusing on a wide range of applications in nondestructive evaluation. Each session took around 30 minutes, and none of the users reported discomfort using the system. We observed the experts during their session. After a completion of a task, we asked the expert users questions regarding the interaction scheme, and we encouraged an open-ended discussion of potential improvements. We report our observations of each session and provide users' feedback.

In the evaluation, we used a laptop equipped with Intel i9-1088H @ 2.4 GHz processor, 64 GB RAM, and Nvidia Quadro RTX 3000 (6 GB VRAM) graphics card. We used the HTC Vive (1080x1200 @ 90 Hz per eye) headset and its two tracked wands in a 2x3 m space.

7.1 Datasets

Three datasets were used in the evaluation: Truss, Honeycomb, and Synthetic truss (Table 1). The Truss dataset is 9x9x9 octet lattice printed by a laser powder bed fusion. The Honeycomb dataset (Fig. 6) is made by direct metal laser sintering with defects purposely placed at known locations. The local defects consist of a crack, missing layer of material, and partially missing layer of material. This dataset serves as a validation case for the scanning and inspection techniques. The experts have previously worked with the Truss and Honeycomb datasets. Lastly, we created a 8x8x8 octet lattice (Synthetic truss) that contains five common local defects (Fig. 5), and constructed a volume with a CT simulator [6]. The local defects are dross, missing strut, broken strut, bent strut, and thin strut (Fig. 1).

7.2 Case Study 1: CAD-to-Scan Registration of an Octet Truss Structure

All experts agreed that the registration of the CAD model to the scan is major bottleneck in the effective analysis of defects. They cited limited depth perception, the difficulty of 2D interactions and the large scans and high polygon count as main reasons why they were not able to achieve this goal with desktop-based approaches.

Table 1: The datasets used in the expert evaluation of the VR system. The Truss and the Honeycomb datasets are additively manufactured, and the Synthetic truss dataset is simulated. 1 GB = 1024^3 bytes.

Dataset	CAD	CT	
	# triangles	Resolution	Size (GB)
Truss	0.9 M	2900x2900x2600	87.5
Honeycomb	3.4 M	1407x389x1388	2.8
Synthetic truss	2.3 M	1200x1200x1200	6.4

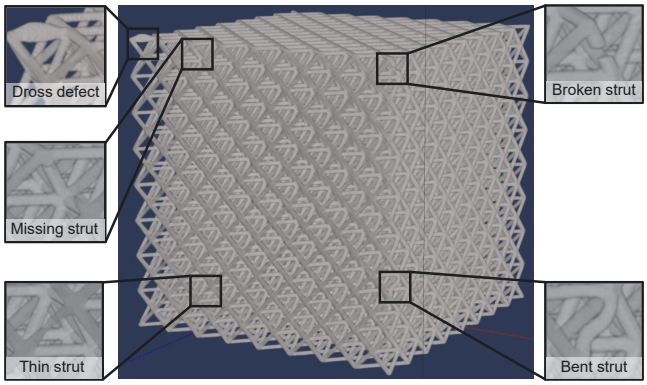

Figure 5: The Synthetic truss dataset with five manually placed defects at known locations used for validation purposes. All defects are placed on the front side of the truss and capture the common defect types.

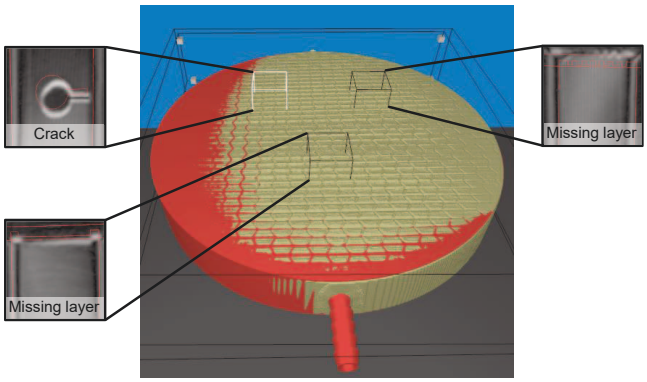

Figure 6: The CAD model (red) of Honeycomb aligned to the CT scan of the manufactured part (visualized with gold isosurface) and the three placed defects. The defect box slices (insets) show the gradient magnitude alongside a contour of the slice-CAD intersection (red). The full-resolution display in the defect box is especially needed for the missing layer of material type of defects.

We decided to use the 9x9x9 octet Truss that is familiar to the experts. For this case study, our goal was to understand how well the experts can understand the spatial structure and align the CAD model with the scan. The units of the CAD model differs from those of the CT object, and it is therefore necessary to be able to adjust object scale. A good fit is assessed by inspecting the objects from various viewing angles. The final step is to deform the CAD model to improve the fit by dragging the eight control points of the deformation mesh.

Overall, the experts agreed that the main benefit of performing this case study in VR is that manipulation comes naturally and the inspection is intuitive. The experts could not compare our system to a desktop-based approach, since they do not have access to one. However, they were all able to quickly achieve an approximate alignment of the CAD model to the isosurface of the CT scan. They confirmed that this task is unquestionably fast and easy to perform in the VR environment (G-3). One expert identified an issue with the selection of overlapping objects, where the controller resolves the selection in a predetermined order, first CAD model, then CT isosurface. After the approximate alignment, all users adjusted the control points of the deformation mesh. They liked the fine manipulation of control points to improve the alignment of the CAD to the CT isosurface. None of the experts raised any issues with the application of dampening to the control point movement, used to reduce the impact of the natural slight hand movements.

At the end of this task, all experts achieved a CAD-to-Scan Registration under ten minutes. However, the result varied in precision of the registration. One expert noted that better precision can be obtained by spending more time at it. The nondestructive evaluation expert suggested the initial alignment can be achieved by adding a capability to place pairs of correspondence points and then using least squares. The primary challenge is the design of an intuitive interaction because the trigger button is now mapped to object manipulation. Another challenge is if the 'solve' step is triggered early, the deformation can be severe, rendering the tool unusable. We expect the point placement will be easier in VR than on a desktop.

At the time of evaluation, we allowed the experts to adjust the isovalue only at the startup of the system. Several users asked if they could adjust the isovalue while using the system. Hence, we added the capability to adjust an isovalue inside the defect box. Overall, the experts agreed that the result of a CAD-to-Scan Registration will have a high impact in their general validation workflow (G-2) because the inspection for defects is simplified to a direct comparison of superimposed surfaces.

7.3 Case Study 2: Local Defect Inspection of Truss and Honeycomb Structures

The second use case is to inspect a part for local defects by selecting an active Defect Box via the minimap after CAD-to-Scan Registration. For this case study, we used the Synthetic truss (8x8x8 octet) and Honeycomb. Both contain local defects that are deliberately placed inside the structure. Three experts were inspecting both datasets, whereas one expert was inspecting only the Truss dataset.

We expected this task to take considerable time because the current desktop visualization tools are used for dozens of hours. Since the defects can be subtle, the portion of the dataset around a defect needs to be viewed at full resolution, and the Defect Box serves this purpose. Interestingly, the first intuition of the users was to scale up the scan so that they were immersed inside. The experts commented that the analysis in VR enabled them to visualize and interact with the scan and CAD model in ways, which was not possible for them before (G-1). They were impressed by the immersion and the ability to look at the structure closely. Although seemingly impressive, the utility for inspecting defects is low. One expert pointedly noted that one quickly loses the sense of orientation while being inside the object and switched back to using the registered CAD-to-scan as minimap. Boxes are placed around the local defects, and we asked the expert users questions covering the manipulation of the slice (orientation and thickness), the comparison approach, and navigation between different boxes. The users navigated easily between the boxes using the defect minimap. Several users would like to define and move a box inside the minimap to explore the data at full resolution or explore the vicinity of a defect.

One aspect where our initial assumption was confirmed was the use of familiar slice views to inspect a local defect at full resolution. In their existing workflow, slices are axis-aligned whereas our VR system enables arbitrary angles. The experts were at first surprised by this additional degree of freedom; however, they got used to it quickly. In the Truss dataset, the experts were surprised that the dataset and mesh loaded almost instantly (due to our multiresolution loading), since the CAD model has a high polygonal count and the scan is tens of gigabytes in size (G-1). The experts stressed that the ability to localize the defect inspection is a large improvement over the usage of slice views of the entire volume. Although we did not task them to look for all defects, they were all able to inspect for the defects they were looking for. The advantage of our system is that the slicing provides essentially the same features as they are used to, but additional augmentations of slice, such as the registered CAD

(a) Lineout measurement. (b) Length measurement.

Figure 7: Screenshots from the expert applying the lineout approach and length measurement.

model intersection, provide enhanced analysis capability and were appreciated by the experts. However, experts wanted to adjust the contrast of the slices, preferably using an automatic method. The design of an intuitive interface to manipulate the contrast would be challenging in itself.

7.4 Case Study 3: 3D Metrology of Truss Structures

Two experts were involved in the evaluation of the 3D Metrology of Truss Structures. We loaded the 9x9x9 Truss and the 8x8x8 Synthetic truss. The measurements of these truss structures are important to quantify their overall defect rate and quality. Measurements usually are performed on the individual struts, which can suffer from common defects (Sect. 7.1). We are interested in the interaction with measurement tools and approximate measurements.

The first expert was primarily using the length measurement approach, as this is the most commonly applied metrology method. By pressing the *Tools* button, the three measurements are displayed as manipulatable objects (Fig. 7). They were immediately able to understand to grab the objects and place them at the target location. The second expert quantified the gap of the broken strut and the size of the dross defect using the length measurement approach (Fig. 7). This expert preferred to measure on the isosurface, and one issue was placing the manipulation points inside the surface due to visibility issues. Although this expert preferred the straightforward measurement on the isosurface, they acknowledged that for certain metrology applications, a slice has to be used. As there were no defects associated with angle deviations, the experts tested the angle measuring approach by confirming the strut orientation in the octet truss. Finally, the lineout approach was applied to obtain the density profile along the dross defect. One issue raised here was that the profile curve is difficult to see due to its color and line thickness. Another problem was the font color, which is the same as the background color on the slice. Both experts were able to perform the measurements in a few minutes. The placement of the start and end manipulation points was straightforward with the controller. However, in some cases, the experts had to readjust the local slice in the Defect Box. Although they were convinced of the utility of performing measurements in VR, they suggested adding the ability to create an inspection report. This report could range from simple screenshots to the extraction of subvolumes augmented with the measurements. Overall, the experts confirmed that using the 3D Metrology approach on the local Defect Box is very fast and intuitive and that they are able to quantify features and defects (G-4), which they confirmed is a key task for validating the scans (G-2).

7.5 Discussion

All participating experts stated that they were impressed with the smoothness and intuitiveness of the VR system. Even as a research prototype, they confirmed that this system enables unprecedented analysis capabilities and opens up new ways to qualify parts. We are currently collaborating with the experts to install a permanent VR inspection space within their facility. On one hand, this installation gives them the ability to test our approach for more scenarios; however, we still need to integrate more features that go beyond a research prototype. On the other hand, this setup will give us the ability to receive feedback from users during actual usage scenarios. We summarize the experts' feedback and our observations.

Consistent Interaction. We observed that consistent interaction metaphor and visual/haptic feedback are crucial to usability. Users were confused if the same manipulation metaphor did not apply to all objects. For example, initially the defect box could not be moved in space, and the slice in the defect box was tied to the orientation and position of a controller. In the next iteration, we made both the defect box and slice behave as regular objects. Further evaluation is necessary to determine if the slice should be moved with the defect box or stay in the same position. Moreover, the experts highlighted the usefulness of the haptic feedback when scrolling on the trackpad to adjust the thickness of the clipped CAD and CT around the slice. Based on this feedback, we added haptic feedback for all selections in the system to accompany the visual highlighting of the bounding boxes already present.

Occlusion, Contrast, and Robustness. Measurements may be obscured by the measured object. For example, the displayed text or graph of lineout may be behind an isosurface. Furthermore, we noticed the issue of contrast of rendered text with respect to the slice view. If the slice is dark, users had difficulty reading text and had to change their head position so the text was displayed against the blue background or gold isosurface. Lastly, users have a significant amount of freedom to place objects and move in the space, potentially causing unexpected issues. One example is the lineout graph, where if a user performs the measurement vertically, the graph is severely distorted.

Integration with Existing Workflows. The experts highlighted the need to record the inspection session for a replay by another user. For example, a technician can annotate defects and record viewpoints that are passed to the material scientist designing the CAD model. In general, inspection reports need to support different levels of abstraction: a detailed report for the scientists and a high-level report for project leaders. Lastly, virtual reality systems are still not widely available, and thus the report needs to be accessible by desktop users. Moreover, the system needs to integrate with existing desktop tools that may be more suitable for some parts of the analysis, especially where keyboard shortcuts and many widgets are needed. Furthermore, the output of the alignment from VR may be used to compute global statistics, e.g., an average truss width.

Generalizability to Other Domains. Our approach is applicable to different scenarios, where we need to analyze a spatial object with respect to an idealistic model. The application we are starting to explore is nondestructive evaluation methods that acquire surface information directly instead of CT scanning. Our approach would be directly applicable to a comparison between the surface of the scanned surface and the designed object (G-2, G-3, G-4). In such a scenario, the CAD-to-Scan Registration could be applied without any changes. However, we would need to replace the slice view in the Defect Box with a clipping plane to provide a similar functionality. As imaging modalities increase in resolution, we can also find applications in the medical domain, especially in the investigation of brain lesions because lesions are often small in comparison to the entire dataset. We could apply the Defect Box approach, where the anatomical atlas corresponds to our CAD model.

8 Limitations

The limitations of the proposed approach are technical and conceptual. On a technical level, the VR system was realized on tethered head-mounted display. The current standalone devices do not have the necessary capacity or rendering performance to handle CAD models containing millions of triangles or CT scans of hundreds of gigabytes. We use a predefined number of MFEM elements to

represent the deformation mesh. During a VR inspection of the Honeycomb dataset, we observed that the thickness of the top and bottom lids differs from the thickness in the input CAD model, requiring stretching deformation, but only of the lids. Placing more MFEM control points would resolve the issue. Another approach would be to dynamically insert control points as needed. A middle ground would be a two-level MFEM mesh, the first level for quick user interaction, and the second level for the offline registration to perform fine adjustments. Additional work is needed to address the inspection of internal structures because viewing inside the complex truss structures is challenging. Space warping techniques, such as obstruction-free lensing [46] or disocclusion headlight [48], may be adapted to preserve the angles and distances, or a world-in-miniature approach [52] could be used to navigate inside truss structures.

On a conceptual level, we focus on those tasks that are difficult to achieve on a desktop. When using the system, our collaborators wanted to access features they are used to from the desktop, such as an overlaid coordinate system, axis-aligned slicing through the entire volume, and exporting image and video material. Although we do not intend to reimplement existing desktop solutions, we will work on creating a data interface between the desktop system and VR system. We noticed that the spatial degree of freedom causes involuntary movements when aligning objects because the user holds the controller in the air without support. We already dampen the movement of the deformation mesh control points and would like to apply this dampening to other manipulations. We will also explore a zoomed-in lens where the controller motion is more precise. Despite highlighting the subset of the data in a defect box, identifying low contrast defects is challenging and time-consuming. Small-scale defects, such as cracks or missing material layers in the Honeycomb dataset, are especially hard to find. However, this problem is not specific to our approach. We plan to try automatic slice placement to highlight defects. If many defects are present, a user will be overwhelmed. Defects will need to be categorized and ranked by their severity to help a user select defects of greatest interest.

9 Conclusion

We facilitate consumer virtual reality technology to demonstrate an efficient and intuitive inspection of highly complex metal additive manufactured parts. Using natural human interfaces, stereoscopic vision, and six degrees of freedom of head and controller movements, we address the bottlenecks in the analysis of deviations of as-built from as-designed. Our defect visualization approach, which uses a low-resolution defect minimap and full-resolution Defect Box, overcomes the challenge of large-scale-volume analysis.

We conducted a user study with four domain experts. We evaluated the usability of the proposed VR system for registration, navigation, and defect inspection. All experts found the tool intuitive and effective, proposed improvements to the tool, and recommended a follow-up study with material scientists who could benefit from our system. They suggested improvements, from adding tools for measuring area and volume to the ability record sessions and create inspection reports.

In the future, we will add an offline registration approach after fine adjustment of the deformation mesh to improve registration. Similar to biology data with semantic information available [20], we could extract the meta-information from the programs that generated the CAD model, and use this information to annotate the CAD mesh and the registered scan. For example, we could number the truss cells on all three axes.

Acknowledgments

The authors wish to thank reviewers, Chuck Divin, Michael Skeate, John Holmen, and Christine Pickett. We thank Hyojin Kim from LLNL for letting us use his X-ray and neutron simulation framework. This work was supported by the US DOE LLNL-LDRD 20-SI-001 and was performed under the auspices of the U.S. Department of Energy by Lawrence Livermore National Laboratory under Contract DE-AC52-07NA27344 (LLNL-CONF-830547). This work was supported in part by NSF OAC awards 2127548, 1941085, 2138811 NSF CMMI awards 1629660, DoE award DE-FE0031880, and the Intel Graphics and Visualization Institute of XeLLENCE, and oneAPI Center of Excellence.

References

[1] nTopology: Next-generation design & engineering software. `https://ntopology.com`, 2021.

[2] OpenViSUS visualization project. `https://github.com/sci-visus/OpenVisus`, 2021.

[3] R. Anderson, J. Andrej, A. Barker, J. Bramwell, J.-S. Camier, J. Cerveny, V. Dobrev, Y. Dudouit, A. Fisher, T. Kolev, W. Pazner, M. Stowell, V. Tomov, I. Akkerman, J. Dahm, D. Medina, and S. Zampini. MFEM: A modular finite element methods library. *Computers & Mathematics with Applications*, 81:42–74, 2021. Development and Application of Open-source Software for Problems with Numerical PDEs.

[4] D. Boges, C. Calí, P. J. Magistretti, M. Hadwiger, R. Sicat, and M. Agus. Virtual environment for processing medial axis representations of 3D nanoscale reconstructions of brain cellular structures. In *25th ACM Symposium on Virtual Reality Software and Technology*, VRST '19. Association for Computing Machinery, New York, NY, USA, 2019.

[5] D. Canepa-Talamas, A. Nassehi, and V. Dhokia. Innovative framework for immersive metrology. *Procedia CIRP*, 60:110–115, 2017. Complex Systems Engineering and Development Proceedings of the 27th CIRP Design Conference Cranfield University, UK 10th – 12th May 2017.

[6] K. M. Champley, T. M. Willey, H. Kim, K. Bond, S. M. Glenn, J. A. Smith, J. S. Kallman, W. D. Brown, I. M. Seetho, L. Keene, S. G. Azevedo, L. D. McMichael, G. Overturf, and H. E. Martz. Livermore tomography tools: Accurate, fast, and flexible software for tomographic science. 126:102595.

[7] C. Christensen, J.-W. Lee, S. Liu, P.-T. Bremer, G. Scorzelli, and V. Pascucci. Embedded domain-specific language and runtime system for progressive spatiotemporal data analysis and visualization. In *2016 IEEE 6th Symposium on Large Data Analysis and Visualization (LDAV)*, pp. 1–10, 2016.

[8] X. Chu, X. Xie, S. Ye, H. Lu, H. Xiao, Z. Yuan, Z. Chen, H. Zhang, and Y. Wu. Tivee: Visual exploration and explanation of badminton tactics in immersive visualizations. *IEEE Transactions on Visualization and Computer Graphics*, pp. 1–1, 2021.

[9] C. Cruz-Neira, D. J. Sandin, T. A. DeFanti, R. V. Kenyon, and J. C. Hart. The CAVE: Audio visual experience automatic virtual environment. *Commun. ACM*, 35(6):64—-72, June 1992.

[10] M. El Beheiry, C. Godard, C. Caporal, V. Marcon, C. Ostertag, O. Sliti, S. Doutreligne, S. Fournier, B. Hajj, M. Dahan, and J.-B. Masson. DIVA: Natural navigation inside 3D images using virtual reality. *Journal of Molecular Biology*, 432(16):4745–4749, 2020.

[11] N. Elmqvist and P. Tsigas. A taxonomy of 3D occlusion management for visualization. *IEEE Transactions on Visualization and Computer Graphics*, 14(5):1095–1109, 2008.

[12] B. Fröhlich, G. Grunst, W. Krüger, and G. Wesche. The Responsive Workbench: A virtual working environment for physicians. *Computers in Biology and Medicine*, 25(2):301–308, 1995. Virtual Reality for Medicine.

[13] W. N. Griffin, W. L. George, T. J. Griffin, J. G. Hagedorn, M. Olano, S. G. Satterfield, J. S. Sims, and J. E. Terrill. Application creation for an immersive virtual measurement and analysis laboratory. In *2016 IEEE 9th Workshop on Software Engineering and Architectures for Realtime Interactive Systems (SEARIS)*, pp. 1–7, 2016.

[14] G. Guennebaud, B. Jacob, et al. Eigen v3. http://eigen.tuxfamily.org, 2010.

[15] U. Günther, T. Pietzsch, A. Gupta, K. I. Harrington, P. Tomancak, S. Gumhold, and I. F. Sbalzarini. scenery: Flexible virtual reality visualization on the Java VM. In *2019 IEEE Visualization Conference (VIS)*, pp. 1–5, 2019.

[16] J. G. Hagedorn, J. P. Dunkers, S. G. Satterfield, A. P. Peskin, J. T. Kelso, and J. E. Terrill. Measurement tools for the immersive visualization

environment: Steps toward the virtual laboratory. *Journal of research of the National Institute of Standards and Technology*, 112(5):257–270.
[17] Y.-J. Huang, T. Fujiwara, Y.-X. Lin, W.-C. Lin, and K.-L. Ma. A gesture system for graph visualization in virtual reality environments. In *2017 IEEE Pacific Visualization Symposium (PacificVis)*, pp. 41–45, 2017.
[18] C. Hurter, N. H. Riche, S. M. Drucker, M. Cordeil, R. Alligier, and R. Vuillemot. FiberClay: Sculpting three dimensional trajectories to reveal structural insights. *IEEE Transactions on Visualization and Computer Graphics*, 25(1):704–714, 2019.
[19] D. Kim, H. Kye, J. Lee, and Y.-G. Shin. Confidence-controlled local isosurfacing. *IEEE Transactions on Visualization and Computer Graphics*, 27(1):29–42, 2021.
[20] D. Kouřil, L. Čmolík, B. Kozlíková, H.-Y. Wu, G. Johnson, D. S. Goodsell, A. Olson, M. E. Gröller, and I. Viola. Labels on levels: Labeling of multi-scale multi-instance and crowded 3D biological environments. *IEEE Transactions on Visualization and Computer Graphics*, 25(1):977–986, 2019.
[21] O. Kreylos. *Interactive visualization and computational steering*. PhD thesis, University of California, Davis, 2003.
[22] O. Kreylos. Environment-independent VR development. In *Advances in Visual Computing*, pp. 901–912. Springer Berlin Heidelberg, 2008.
[23] O. Kreylos, E. W. Bethel, T. J. Ligocki, and B. Hamann. Virtual-reality based interactive exploration of multiresolution data. In *Hierarchical and Geometrical Methods in Scientific Visualization*, pp. 205–224. Springer Berlin Heidelberg, Berlin, Heidelberg, 2003.
[24] O. Kreylos, N. Max, B. Hamann, S. Crivelli, and E. Wes Bethel. Interactive protein manipulation. In *IEEE Visualization, 2003. VIS 2003.*, pp. 581–588, 2003.
[25] O.-H. Kwon, C. Muelder, K. Lee, and K.-L. Ma. A study of layout, rendering, and interaction methods for immersive graph visualization. *IEEE Transactions on Visualization and Computer Graphics*, 22(7):1802–1815, 2016.
[26] B. Laha, D. A. Bowman, and J. J. Socha. Effects of VR system fidelity on analyzing isosurface visualization of volume datasets. *IEEE Transactions on Visualization and Computer Graphics*, 20(4):513–522, Apr. 2014.
[27] B. Laha, K. Sensharma, J. D. Schiffbauer, and D. A. Bowman. Effects of immersion on visual analysis of volume data. *IEEE Transactions on Visualization and Computer Graphics*, 18(4):597–606, 2012.
[28] B. Lee, D. Brown, B. Lee, C. Hurter, S. Drucker, and T. Dwyer. Data visceralization: Enabling deeper understanding of data using virtual reality. *IEEE Transactions on Visualization and Computer Graphics*, 27(2):1095–1105, 2021.
[29] M. J. Lobo, C. Hurter, and P. Irani. Flex-ER: A platform to evaluate interaction techniques for immersive visualizations. *Proc. ACM Hum.-Comput. Interact.*, 4(ISS), Nov. 2020.
[30] W. E. Lorensen and H. E. Cline. Marching cubes: A high resolution 3D surface construction algorithm. *SIGGRAPH Comput. Graph.*, 21(4):163—169, Aug. 1987.
[31] T. Maconachie, M. Leary, B. Lozanovski, X. Zhang, M. Qian, O. Faruque, and M. Brandt. SLM lattice structures: Properties, performance, applications and challenges. *Materials & Design*, 183:108137, Dec. 2019.
[32] M. Mazur, M. Leary, S. Sun, M. Vcelka, D. Shidid, and M. Brandt. Deformation and failure behaviour of Ti-6Al-4V lattice structures manufactured by selective laser melting (SLM). *The International Journal of Advanced Manufacturing Technology*, Sept. 2015.
[33] R. C. Mota, A. Rocha, J. D. Silva, U. Alim, and E. Sharlin. 3De interactive lenses for visualization in virtual environments. In *2018 IEEE Scientific Visualization Conference (SciVis)*, pp. 21–25. IEEE, 2018.
[34] U. Obeysekare, C. Williams, J. Durbin, L. Rosenblum, R. Rosenberg, F. Grinstein, R. Ramamurti, A. Landsberg, and W. Sandberg. Virtual Workbench - a non-immersive virtual environment for visualizing and interacting with 3D objects for scientific visualization. In *Proceedings of Seventh Annual IEEE Visualization '96*, pp. 345–349, 1996.
[35] V. Pascucci and R. J. Frank. Global static indexing for real-time exploration of very large regular grids. In *Proceedings of the 2001 ACM/IEEE Conference on Supercomputing*, SC '01, p. 2. Association for Computing Machinery, New York, NY, USA, 2001.
[36] S. Pidhorskyi, M. Morehead, Q. Jones, G. A. Spirou, and G. Doretto. syGlass: Interactive exploration of multidimensional images using virtual reality head-mounted displays. *CoRR*, abs/1804.08197, 2018.
[37] Prabhat, A. Forsberg, M. Katzourin, K. Wharton, and M. Slater. A comparative study of desktop, fishtank, and cave systems for the exploration of volume rendered confocal data sets. *IEEE Transactions on Visualization and Computer Graphics*, 14(3):551–563, 2008.
[38] B. Preim, C. Tietjen, W. Spindler, and H.-O. Peitgen. Integration of measurement tools in medical 3d visualizations. In *IEEE Visualization, 2002. VIS 2002.*, pp. 21–28, 2002.
[39] K. Reda, A. Knoll, K. Nomura, M. E. Papka, A. E. Johnson, and J. Leigh. Visualizing large-scale atomistic simulations in ultra-resolution immersive environments. In *2013 IEEE Symposium on Large-Scale Data Analysis and Visualization (LDAV)*, pp. 59–65. IEEE Computer Society, Los Alamitos, CA, USA, Oct. 2013.
[40] B. Reitinger, D. Schmalstieg, A. Bornik, and R. Beichel. Spatial analysis tools for virtual reality-based surgical planning. In *3D User Interfaces (3DUI'06)*, pp. 37–44, 2006.
[41] G. Roberts, N. Holmes, N. Alexander, E. Boto, J. Leggett, R. M. Hill, V. Shah, M. Rea, R. Vaughan, E. A. Maguire, K. Kessler, S. Beebe, M. Fromhold, G. R. Barnes, R. Bowtell, and M. J. Brookes. Towards OPM-MEG in a virtual reality environment. *NeuroImage*, 199:408–417, 2019.
[42] J. Schindelin, I. Arganda-Carreras, E. Frise, V. Kaynig, M. Longair, T. Pietzsch, S. Preibisch, C. Rueden, S. Saalfeld, B. Schmid, J.-Y. Tinevez, D. J. White, V. Hartenstein, K. Eliceiri, P. Tomancak, and A. Cardona. Fiji: an open-source platform for biological-image analysis. *Nature Methods*, 9(7):676–682, 2012.
[43] D. Shidid, M. Leary, P. Choong, and M. Brandt. Just-in-time design and additive manufacture of patient-specific medical implants. *Physics Procedia*, 83:4–14, 2016.
[44] M. Sousa, D. Mendes, S. Paulo, N. Matela, J. Jorge, and D. S. o. Lopes. VRRRRoom: Virtual reality for radiologists in the reading room. In *Proceedings of the 2017 CHI Conference on Human Factors in Computing Systems*, CHI '17, pp. 4057—-4062. Association for Computing Machinery, New York, NY, USA, 2017.
[45] C. Tominski, S. Gladisch, U. Kister, R. Dachselt, and H. Schumann. Interactive lenses for visualization: An extended survey. *Computer Graphics Forum*, 36(6):173–200, 2017.
[46] M. Traoré, C. Hurter, and A. Telea. Interactive obstruction-free lensing for volumetric data visualization. *IEEE Transactions on Visualization and Computer Graphics*, 25(1):1029–1039, 2019.
[47] W. Usher, P. Klacansky, F. Federer, P.-T. Bremer, A. Knoll, J. Yarch, A. Angelucci, and V. Pascucci. A virtual reality visualization tool for neuron tracing. *IEEE Transactions on Visualization and Computer Graphics*, 24(1):994–1003, 2018.
[48] L. Wang, J. Chen, Q. Ma, and V. Popescu. Disocclusion headlight for selection assistance in VR. In *2021 IEEE Virtual Reality and 3D User Interfaces (VR)*, pp. 216–225, 2021.
[49] Y. Wang, Q. Li, L. Liu, Z. Zhou, Y. Wang, L. Kong, N. Zhong, R. Chai, X. Luo, Y. Guo, M. Hawrylycz, Q. Luo, Z. Gu, W. Xie, H. Zeng, and H. Peng. TeraVR empowers precise reconstruction of complete 3-D neuronal morphology in the whole brain. *Nature Communications*, 10(1):3474, 2019.
[50] G. Wyvill, C. McPheeters, and B. Wyvill. Data structure for soft objects. *The Visual Computer*, 2:227–234, 1986.
[51] X. Yang, R. C. Malak, C. Lauer, C. Weidig, H. Hagen, B. Hamann, J. C. Aurich, and O. Kreylos. Manufacturing system design with virtual factory tools. *International Journal of Computer Integrated Manufacturing*, 28(1):25–40, 2015.
[52] Y. Yang, M. Cordeil, J. Beyer, T. Dwyer, K. Marriott, and H. Pfister. Embodied navigation in immersive abstract data visualization: Is overview+detail or zooming better for 3D scatterplots? *IEEE Transactions on Visualization Computer Graphics*, 27(02):1214–1224, feb 2021.
[53] H. Zhou, X. Zhang, H. Zeng, H. Yang, H. Lei, X. Li, and Y. Wang. Lightweight structure of a phase-change thermal controller based on lattice cells manufactured by SLM. *Chinese Journal of Aeronautics*, 32(7):1727–1732, 2019.